Design and Analysis of the Two-Stage FGM-148 Javelin Anti-Tank Missile

by

David Qi Zhang

A Project Submitted to the Graduate

Faculty of Rensselaer Polytechnic Institute

in Partial Fulfillment of the

Requirements for the degree of

MASTER OF ENGINEERING

Approved:

_____

Ernesto Gutierrez-Miravete, Project Adviser

Rensselaer Polytechnic Institute
Hartford, Connecticut

March, 2012
(For Graduation August, 2012)

CONTENTS

LIST OF TABLES

LIST OF FIGURES

LIST OF SYMBOLS

A_b: Burn area, m^2

X^*: X-function

R°: Gas constant, J/kg·K

R: Universal gas constant, 8.3144 J/mol·K

M_w: Molecular weight, kg/kmol

γ: Ratio of specific heats

A_e: Nozzel exit area, m^2

A^*: Throat area, m^2

ε: Expansion ratio

r_b: Burn rate, m/s

P_C: Combustion chamber pressure, Pa

F_N: Motor thrust, N

C_F: Coefficient of thrust

I_{sp}: Specific impulse, s

t_b: Burn time, s

t_{tube}: Time to traverse launch tube, s

$\dot{m}_c$ = Mass flow of combustion chamber, kg/s

$\dot{m}^*$ = Mass flow of throat, kg/s

ρ = Density, kg/m^3

d = Displacement, m

GLOSSARY

ATGM: Anti-Tank Guided Missile

RPG: Rocket Propelled Grenade

HTPB: Hydroxyl-Terminated Polybutadiene

AP: Ammonium Perchlorate

Al: Aluminum

BATES: Ballistic Test and Evaluation System

ACKNOWLEDGMENT

To my parents, who made my engineering education possible. And to all my teachers and friends that encouraged me along the way.

ABSTRACT

This report is an analysis and design of a two-stage anti-tank missile based on the currently fielded FGM-148 Javelin missile. The design and analysis will be broken into three parts: the analysis and design of the launch motor, the flight motor, and aerodynamic effects on the missile while it's in flight. Due to the complexities of aerodynamics in a full, three-axis system, the scope of the project will be limited to a two-dimensional plane (i.e. the missile is tracking a stationary target). To aid in the validation of the design of the motors, the simulation software, BurnSim, will be used.

The goal of will be to design a non-separating, two-stage motor that will be able to launch the missile a sufficient distance to clear the operator of the flight motor's backblast and be able to sustain the missile along its full range, direct attack flight profile.

1. INTRODUCTION

An Anti-Tank Guided Missile (ATGM) is a category of rocket-based weapon that is primarily use against armored vehicles. While rockets in warfare were used as early as the 11th century, they were crude and used more for their psychological effects. The advancement of mechanized, armored warfare during World War II marked the beginning of the rocket's use as a practical anti-armor weapon by the infantry.

These light, man-portable rockets were essentially rocket-propelled grenades (RPG), with no form of guidance other than how the operator pointed the launcher. What allowed them to defeat armor and remain compact was the development of the shaped charge, based on the Munroe effect. These anti-tank rockets generally weighed roughly 1.5 kg and were able to puncture 60 mm of steel plate. As armor developed during the course of the war, the size of the warhead had to be increased to match. By the end of the war, anti-tank rockets were able to penetrate up to 100 mm of armor (Fig. 1).

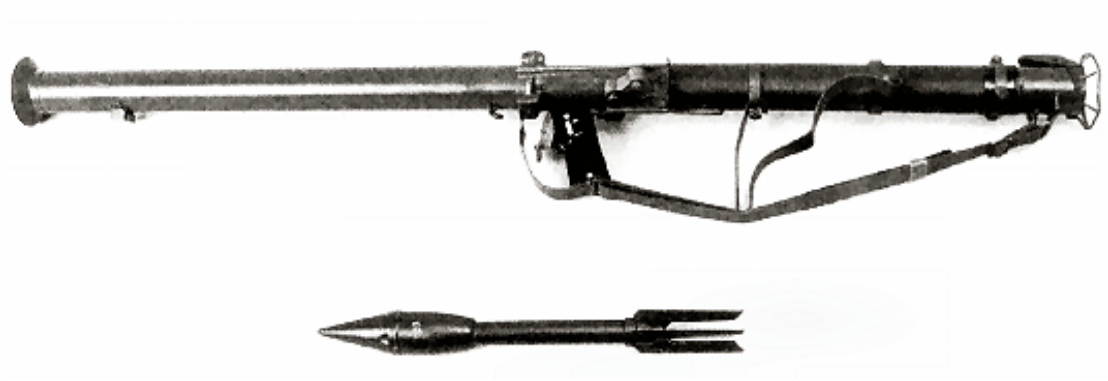

Figure 1: M9A1 Rocket Launcher

Modern armored vehicles deploy a wide array of armor in both composition and shape. In order to defeat this armor, warheads had to increase in both diameter and weight. Concurrent development of microchips meant that guidance computers could now be installed into the rocket to change its trajectory in flight. All systems combined, ATGMs could weigh more than 10 kg and were over 1 m in length. The large backblast of the motor required to propel the rocket into flight meant they were mostly launched from vehicles, where the crew could be protected.

Man-portable ATGMs are still needed as the individual soldier is more agile and readily deployed than vehicles. The solution to allow a soldier to launch these more massive missiles came in the development of a two-stage motor (Fig. 2). The first motor, in what's called a soft launch, produces enough thrust to launch the missile out of the tube and a safe distance away, but was completely burned before the nozzle left the tube, leaving no exhaust to hit the operator. The flight motor would then ignite to propel the ATGM along its attack path.

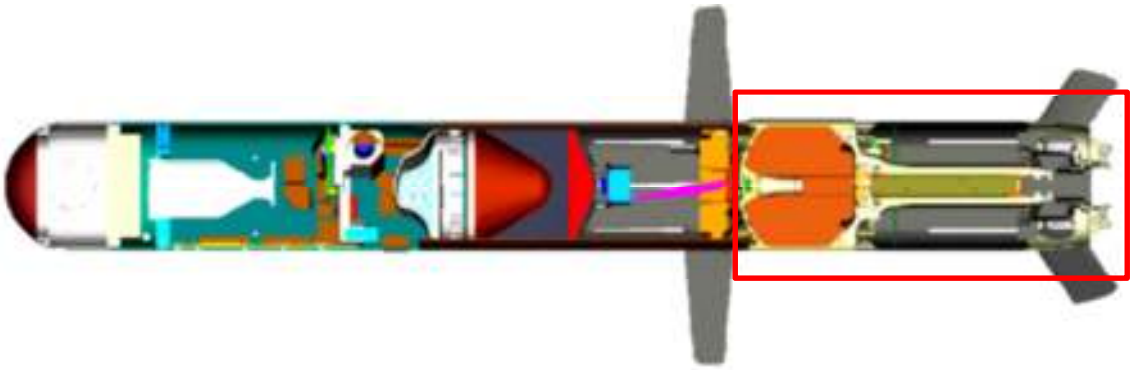

Figure 2: FGM-148 Javelin (Launch/Flight Motors Highlighted)

2. METHODOLOGY

2.1 SOLID MOTOR ROCKET DESIGN

The design of solid fuel motors is essentially based on propellant properties and grain geometry. The spreadsheet tool used for the launch and flight motor design for this project is based off of an example problem [1]. The process is an iterative one, where an initial motor design is assumed to determine the design's performance (usually thrust and burn time). The sizing is then changed accordingly to obtain the performance required.

The first step is to determine the burn area of the motor (Equation 1). The burn area is dependent on if the motor is to be an end burner or radial burner. An end burner will have a constant burn area, whereas a radial burner's varies as the propellant burns.

$$A_b = (burn\ perimeter)\ x\ (charge\ length) \tag{1}$$

The next calculation is the X-function (Equation 2). The X-function is usually calculated with the assumption that the Mach number at the throat is 1.0.

$$X^* = \sqrt{\gamma}\left[\frac{2}{\gamma+1}\right]^{\frac{\gamma+1}{2(\gamma-1)}} \tag{2}$$

The gas constant will also need to be found for the particular propellant (Equation 3).

$$R^\circ = \frac{R}{M_w} \tag{3}$$

For conceptual designs, an expansion ratio (ε) of 4.0 is usually picked. This defines the relationship between the nozzle exit area and the throat area (Equation 4).

$$A^* = \frac{A_e}{\varepsilon} \tag{4}$$

Assuming that the mass flow through the combustion chamber (Equation 5) and the throat (Equation 6) are equivalent (steady flow), the equations can be combined with the burn rate (Equation 7) to obtain the chamber pressure (Equation 8).

$$\dot{m}_c = \rho_P A_b r_b \tag{5}$$

$$\dot{m}^* = \frac{P_C A^* X^*}{\sqrt{RT_C}} \tag{6}$$

$$r_b = \frac{k\left(10^{-5} P_C\right)^n}{1000} \tag{7}$$

$$P_C = \left[\frac{\rho_P A_b k \left(10^{-5}\right)^n \sqrt{RT_C}}{1000 A^* X^*}\right]^{\frac{1}{1-n}} \tag{8}$$

The coefficient of thrust, C_F, is obtained assuming an ideal rocket nozzle: $P_{te} = P_{tc} = P_C$ (Equation 9). In practice, the coefficient of thrust is usually reduced by 10%, $C_{F,actual}$

$$C_F = \sqrt{\frac{2\gamma^2}{\gamma-1}\left[\frac{2}{\gamma+1}\right]^{\frac{\gamma+1}{\gamma-1}}\left[1-\left(\frac{P_e}{P_C}\right)^{\frac{\gamma-1}{\gamma}}\right]} + \frac{A_e}{A^*}\left[\frac{P_e - P_0}{P_C}\right] \tag{9}$$

Finally, thrust can be found as a function of $C_{F,actual}$, P_C, A^* (Equation 10).

$$F_N = C_{F,actual} P_C A^* \tag{10}$$

2.2 KINEMATICS

To determine the parameters needed for the launch motor to propel the missile to the safe minimal distance, the missile was treated as a ballistic projectile problem, starting as a box on a ramp. From the technical specifications of the Javelin missile (Table 1), [2], [3], a simple force diagram was developed to represent the forces that needed to be overcome (Fig. 3).

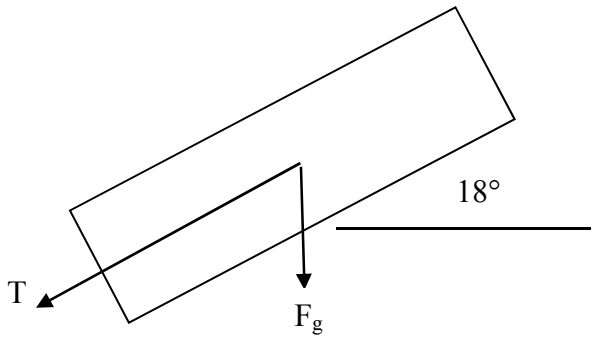

Figure 3: Force Body Diagram

Missile Mass (kg)	Missile Diameter (m)	Tube Length (m)	Missile Range (m)	Motor Burn Time (s)	Flight Time (s)	Max Altitude (m)	Launch Angle (deg)
11.8	.140	1.2	2,000	~6	14	60	18

Table 1: FGM-148 Javelin Specifications [2], [3]

The amount of force required is unknown. An initial guess is required and iterations done until the resultant burn time is acceptable. Newton's Second Law and equations of motion for displacement and velocity were used to obtain a force / time relationship (Equations 11, 12, 13). The acceleration, tube exit velocity, soft launch range, time to travel the tube length can also be found. The force required is equivalent to the thrust the soft launch motor needs to produce. For these calculations, the friction of the graphite / fiberglass tube is taken into account [4], [5].

$$\sum F_x = ma_x$$
$$T - F_{gx} - F_f = ma \tag{11}$$

$$v_f{}^2 = v_i{}^2 + 2ad \tag{12}$$

$$t = \frac{2d}{v_f - v_i} \tag{13}$$

2.3 SOFT LAUNCH MOTOR DESIGN

From a US Army injury report [6], the rough size of the launch motor can be estimated to be about .15 m long (Fig. 4). Propellant properties were obtained from the [7], (Table 2). An HTPB/AP/Al propellant was picked because it contains a low percentage of metal content, especially aluminum, as when it burns, it leaves a visible exhaust trail. Using the spreadsheet tool, the approximate size, and the propellant properties, a motor can be designed. A BATES cylindrical grain cross-section as a radial burner was picked as it is the most common profile and a radial burner is able to produce the most thrust in the shortest period of time. The motor will have to satisfy the conditions found from the kinematics computations. Once a size is found that produces

close to 3,000 N of thrust, the value will be inputted into the kinematics equation to check if the burn time is less than the time it takes to travel the length of the tube.

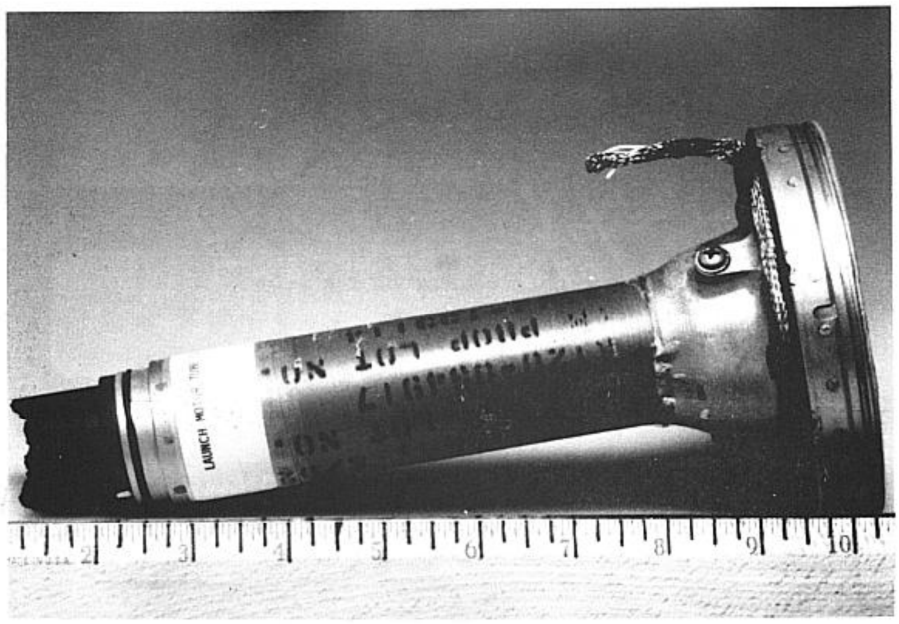

Figure 4: Launch Motor Housing [6]

Density (kg/m^3)	Burn Rate, r_b (cm/s)	n	T_C (K)	C^* (m/s)	M_w	γ
1854.6	7.62	.4	2816	1590	25	1.21

Table 2: HTPB/AP/Al Properties [7]

Once the motor was designed, a FEM analysis has to be performed to ensure that the motor casing is sufficient to withstand the combustion pressure generated by the burning fuel.

The motor casing must also be lined with an insulating material to prevent the combustion heat from burning through. Because of the high temperatures, a graphite (carbon / carbon) liner will be used [8]. Thermal diffusivity (Equation 14) measures how quickly the material transfers heat.

$$\alpha = \frac{k}{\rho C_p} \tag{14}$$

As the launch motor casing is not ejected when it is spent, the insulation will need to withstand the heat for 6 s.

2.4 FLIGHT MOTOR DESIGN

The flight motor is designed in a manner similar to the launch motor. The performance characteristics of the flight motor are known [2], (Table 3). The section cut model of the flight motor from the same report will give approximate dimensions to start the sizing iterations.

Time (s)	Thrust (N)	Mass (kg)
0	0	11.25
.3	570	11.16
.6	650	11.06
1.2	750	10.82
1.8	770	10.58
2.4	650	10.38
4.2	50	10.16
5.2	0	10.15

Table 3: Actual Flight Motor Performance [2]

As the actual propellant composition is classified, the launch motor propellant will be used. This will cause the designed motor to have a slightly different performance than the actual motor.

As with the launch motor, an insulation layer will be added between the propellant and casing. As the propellant is the same in the two motors, the chamber temperature will be the same, resulting in the same thickness. Along with a casing 2.5 mm thick, this will set the maximum outer diameter of the propellant. FEM analysis was also done on the casing to ensure the pressure is not enough to rupture the casing.

2.5 BURST DISK

In order to keep the missile as compact as possible, the launch and flight motors are integrated into a single, overall unit. What allows this to be possible is the use of a burst

disk placed between the two motors [9], shaped in such a way as to be able to resist the launch motor pressure, while rupturing easily when the flight motor is ignited. The actual shape of the disk is unknown, so it will be approximated as, concavo-convex, with the convex side protruding into the launch motor (Fig. 5). This is because a domed surface provides excellent resistance to pressures on the convex side. The material will be .01 m thick 7075-T6 aluminum (Table 4).

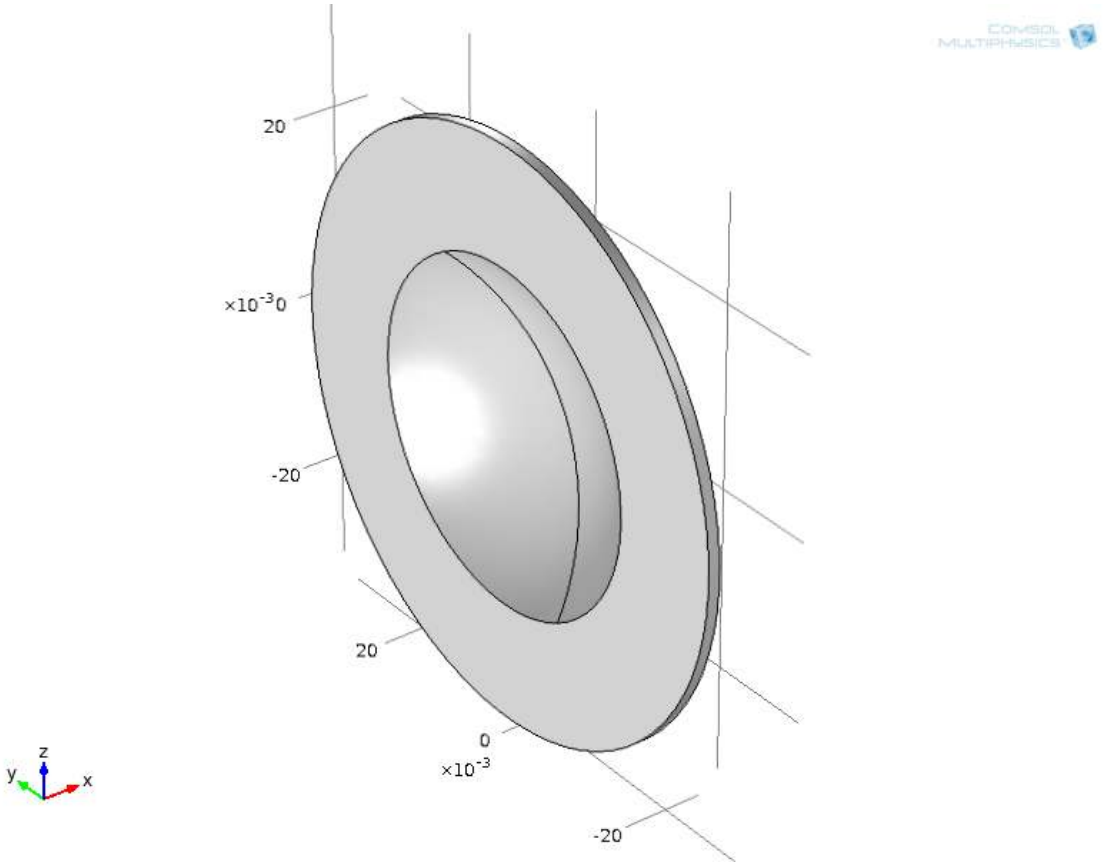

Figure 5: Burst Disk

Young's Modulus (GPa)	Poisson's Ratio	Density (kg/m^3)
68.9	.33	2700

Table 4: 7075-T6 Properties

The more critical aspect to the burst disk is to ensure that it will withstand the launch motor pressure so it will not prematurely rupture and ignite the flight motor. A FEM analysis will be performed with the launch motor pressure against the outer convex face.

2.6 FLIGHT PHASE

The flight profile to design to is the full-range direct attack profile, (Fig. 6), [10]. Compared to the top attack profile, the direct attack is flatter, allowing the assumption to be made that the variation in altitude is negligible compared to the horizontal distance traveled, reducing the kinematics equations (Equations 15, 16) to one axis. From these kinematics equations, the velocity and distance traveled can be numerically computed by a finite difference method.

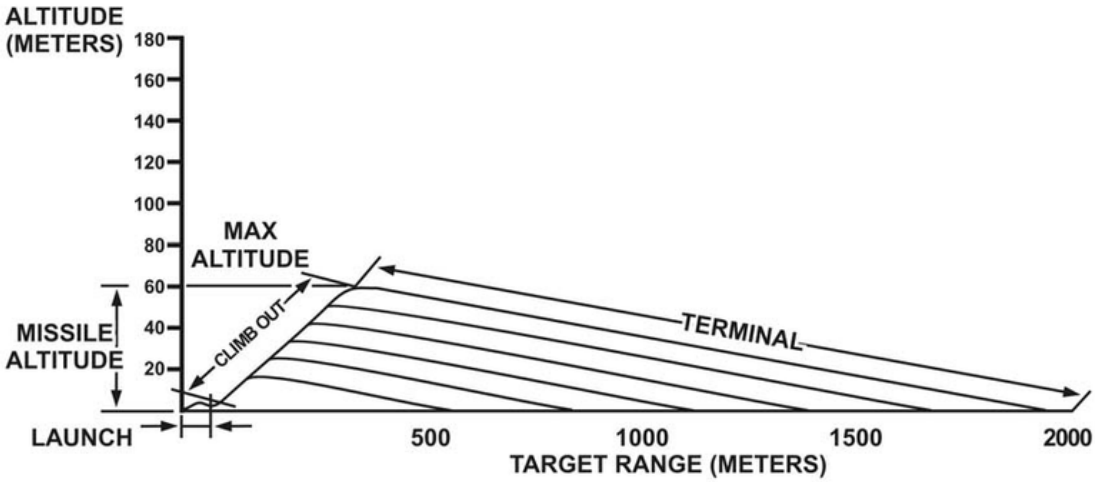

Figure 6: Direct Attack Flight Profile [10]

$$\sum F_x = ma_x$$

$$T - F_D = m_i \frac{v_f - v_i}{t_f - t_i} \tag{15}$$

$$v_i = \frac{x_f - x_i}{t_f - t_i} \tag{16}$$

The Javelin uses eight mid-section wings for stability. The airfoil shape for each of the wings has to be symmetric; otherwise, a cambered airfoil will generate lift even at

the 0° Angle of Attack (AoA) and destabilize the missile as it flies. An example symmetric airfoil is a NACA 0015, which has a Coefficient of Lift (C_l) zero at 0° AoA [11]. From the lift equations (Equation 17), a C_l of zero will cause no lift. Thus, the only forces to take into account are the thrust, drag, and mass. A generic Coefficient of Drag value of .3 is used to determine drag (Equation 18), [2].

$$F_L = \frac{1}{2}\rho C_l A v^2 \tag{17}$$

$$F_D = \frac{1}{2}\rho C_d A v^2 \tag{18}$$

For ease of computation, it is assumed that the density and speed of sound of air is equal to its sea level value up to the height of 60 m [12]. The area to use in the drag equation is the cross sectional area of the body. The cross sectional areas of the mid-body and directional wings are assumed to be insignificant.

3. RESULTS AND DISCUSSION

3.1 KINEMATICS

Assuming ideal conditions, the only force acting on the rocket while inside the tube is its weight along the length of the tube, 66.396 N. Using that as a starting point, along with the equations in Section 2.6, the following results were found (Table 5).

Force (N)	a (m/s^2)	v_{exit} (m/s)	t_{tube} (s)
66.396	-3.469	N/A	N/A
500	32.277	8.937	.269
1000	75.65	13.474	.178
1500	118.023	16.830	.143
2000	160.396	19.620	.122
2500	202.769	22.060	.109
3000	245.141	24.256	.099
3500	287.514	26.269	.091

Table 5: Kinematics

Similar missiles that utilize a soft launch feature accelerated the missile to roughly 25 m/s before the flight motor takes over [13]. Thus, the launch motor will need to produce about 3000 N of thrust.

3.2 SOFT LAUNCH MOTOR DESIGN

The core (area without propellant) diameter is the primary variant in the design, as the length and overall diameter of the propellant and the throat and nozzle diameters are fixed. As the burn rate is a fixed characteristic of the propellant, varying the core diameter results in a change in the combustion pressure and thrust. This also changes the overall burn time, as a smaller core means more propellant to burn through. From this a final launch motor design was obtained (Table 6). Iterating this thrust value in the kinematics equation (Equations 11, 12, 13) results in a t_{tube} of .124 s. This motor is sufficient as it produces enough thrust and burns out before it has finished traveling the length of the tube.

Motor Length (m)	Motor Diameter (m)	Core Diameter (m)	Insulation Thickness (m)	Casing Thickness (m)	Thrust (N)	t_b (s)	t_{tube} (s)
.1524	.0508	.0365	.001	.0025	2,933.424	.122	.124

Table 6: Launch Motor Final Design

The FEM analysis for the housing was done in COMSOL. The material picked was a generic stainless steel (Table 7). The housing was approximated as a cylinder 2.5 mm thick for simplification. The housing was fixed lengthwise at two opposite points along the outside perimeter and the combustion chamber pressure applied along the inside surface.

Young's Modulus	Poisson's Ratio	Density
200 MPa	.3	7850 kg/m^3

Table 7: Stainless Steel Properties

The highest stress the housing experiences is 275.4 MPa. This is well within the yield strength range of stainless steel (Fig. 7).

Pyrolytic graphite is typically used as insulation in rocket motors with a thermal diffusivity is 3.6 x 10^{-6} m^2/s. During the total burn time, the heat will diffuse through 2.16 x 10^{-5} m^2 of insulation. This is the difference in area from the outer diameter to inner diameter (d_{charge}). Knowing to d_{charge} be .0458 m, this gives an insulation thickness of .305 mm. To ensure a large factor of safety, the thickness will be increased to 1 mm even. This increases the total casing diameter to .0578 m.

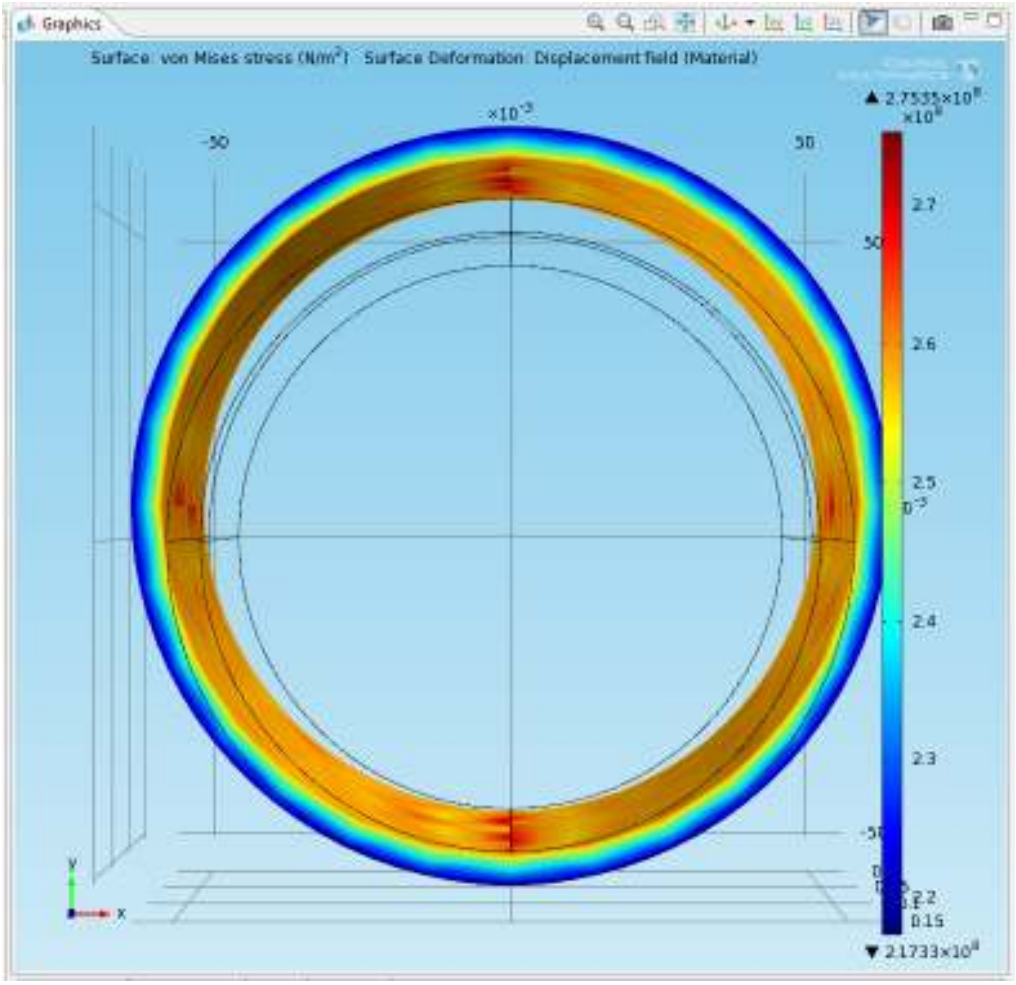

Figure 7: Housing von Mises Stress Distribution

3.3 FLIGHT MOTOR DESIGN

Using the same set of equations and process to design the launch motor, the flight motor final size was found, (Table 8). In order to best match the actual motor performance, the burn rate constant (k) of the propellant was modified to be 2.5 instead of 5.58. Compared to the actual flight motor performance, in terms of thrust and time, it can be seen that they have very different performance profiles, (Table 9), (Fig. 8). From the cross section of the model, the flight motor has a tubular design. However, the data indicates the flight motor performs more like a rod and tube design. Again, the discrepancy can be attributed to the classified propellant. The properties, as well as how

it burns is unknown. The designed motor steadily burns its way to a similar maximum thrust roughly 2 seconds later than the actual motor.

As the insulation was sized to withstand the same propellant's combustion temperature for a duration of 6 seconds, it will be used again to line the casing.

Motor Length (m)	Motor Diameter (m)	Core Diameter (m)	Insulation Thickness (m)	Casing Thickness (m)
.05	.12	.05	.001	.0025

Table 8: Flight Motor Final Design

Time (s)	Thrust (N)	Mass (kg)
0	159.918	10.931
.5	204.269	10.883
1	252.861	10.829
1.5	308.893	10.763
2	373.212	10.686
2.5	446.733	10.595
3	530.437	10.487
3.5	625.375	10.362
4	732.671	10.15

Table 9: Flight Motor Performance

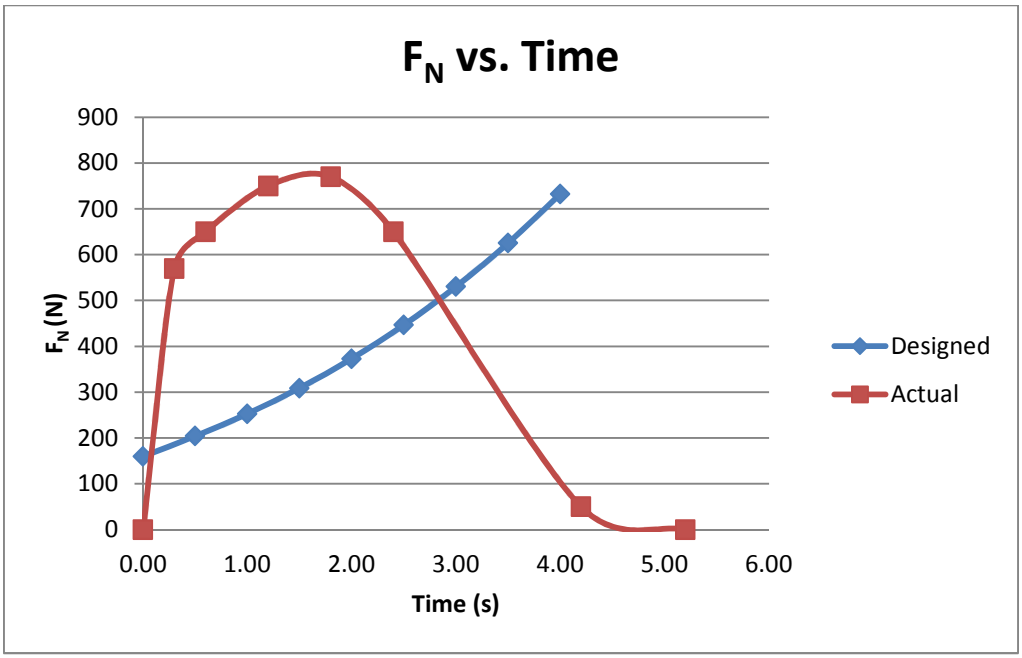

Figure 8: Actual vs. Design Flight Motor Performance

The 3D model of the flight motor casing is more complex than the simple tube approximation of the launch motor. It was found that even a very coarse mesh of the 3D model would result in more than 11,600 elements, which was more than what the computer could handle. As such, a 2D, axisymmetric model was used. The COMSOL plot (Fig. 9) shows that the highest stress on a stainless steel (Table 6) casing of 2.5 mm thick is 369 MPa, which is well under the 502 MPa yield strength of a stainless steel like AISI 302.

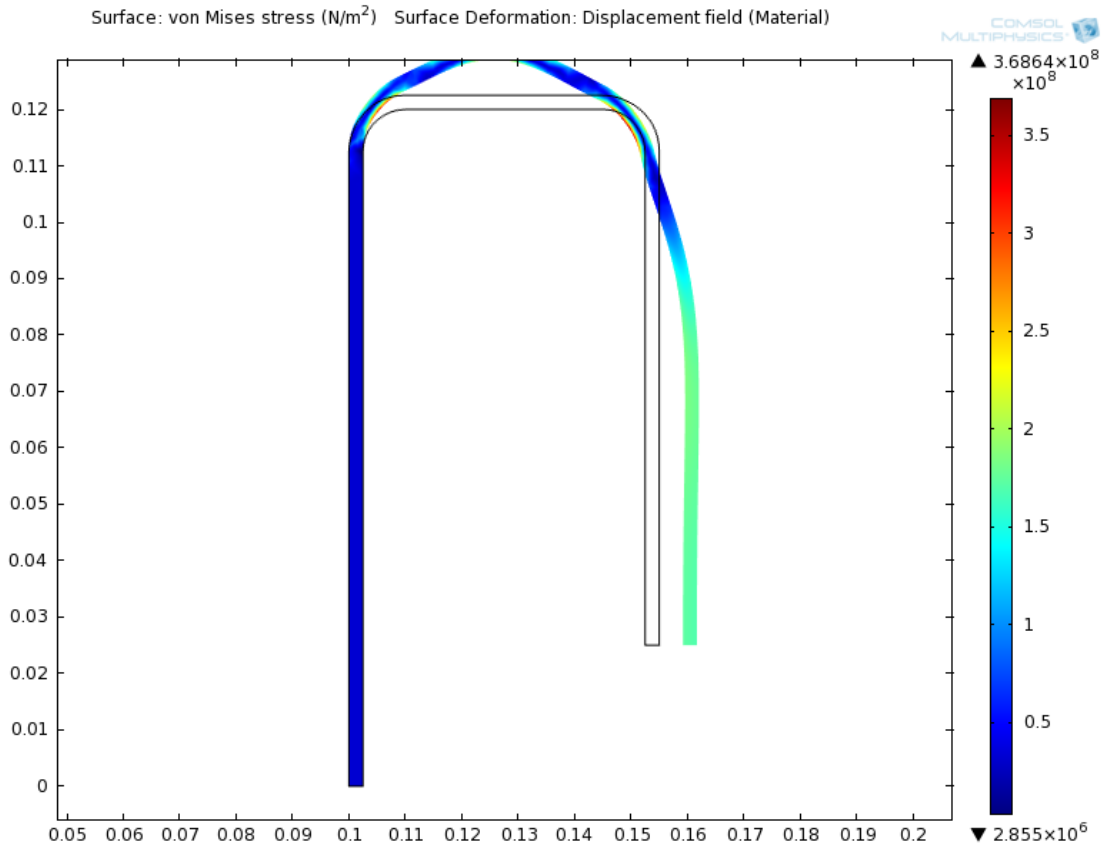

Figure 9: Flight Motor von Mises Stress Distribution

3.4 BURST DISK

With a pressure of 16.3 MPa applied to the outer convex face, the maximum stress the burst disk experiences is 476 MPa, which is right around the yield stress limit of 7075-T6 aluminum (Figure 10). What the plot shows is that the stress concentration will occur at where the disk goes from flat to curved, which ensures that when the disk fails, the opening will not constrict the flow of exhaust gases. The stress being very close to the yield stress of 7075-T6 aluminum also means that the disk has been weakened enough that the force of the flight motor should be enough to rupture the disk.

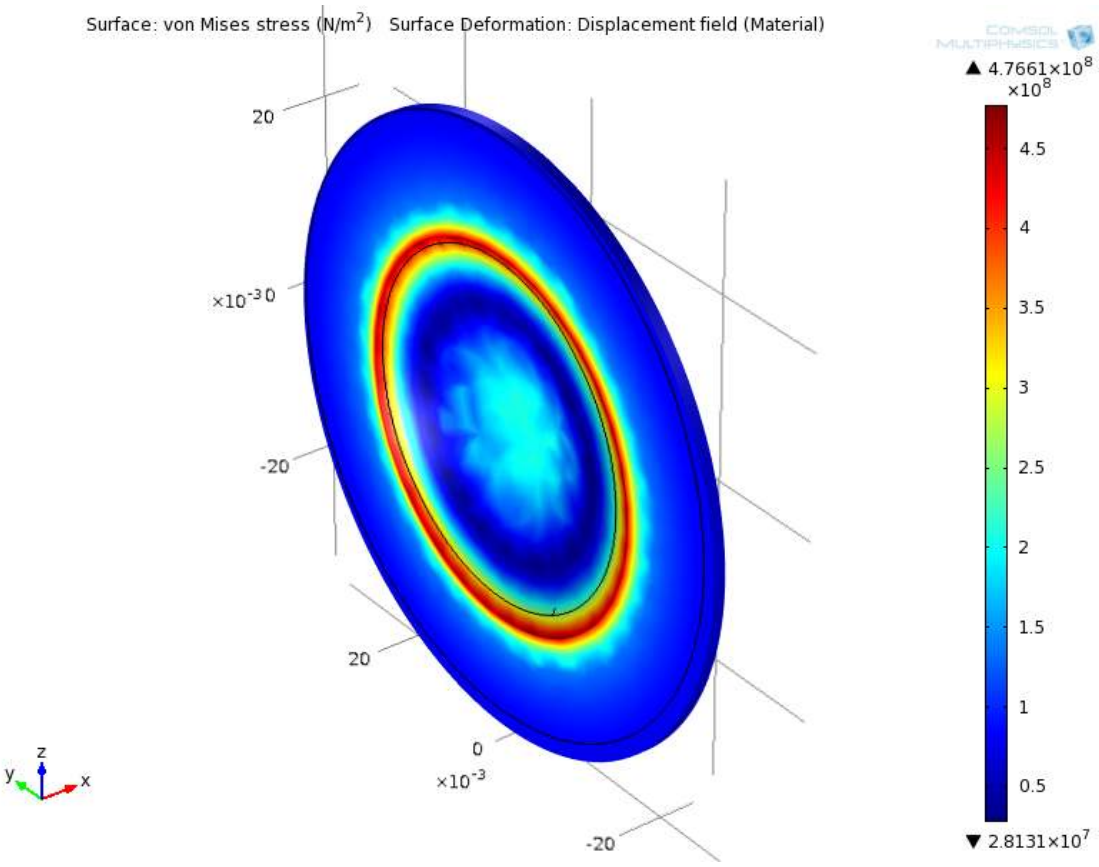

Figure 10: Burst Disk von Mises Stress

3.5 FLIGHT PHASE

Assuming the flight profile consists of two right triangles meeting at the 300 m horizontal mark, the actual distance traveled (lengths of the hypotenuses), was found to be 2007 m. This justifies the reduction of analysis to just the horizontal component. Using the data from Figure 5, and Equations 15 and 16, the velocities and displacements can be found, (Table 10).

Time (s)	Velocity (m/s)	Velocity (M)	Displacement (m)
0	19.412	.057	0
.5	28.793	.085	14.396
1	40.459	.119	34.626
1.5	54.791	.161	62.021
2	72.221	.212	98.132
2.5	93.246	.274	144.755
3	118.439	.348	203.975
3.5	148.459	.436	278.204
4	184.298	.542	370.353
5	183.519	.539	553.872
10	179.721	.528	1460.01
13	177.517	.522	1994.754
14	176.794	.519	2171.549

Table 10: Flight Velocities and Displacement

The velocity the designed missile reaches at 4 seconds is close to the maximum velocity of the actual missile. From the geometric calculation of the flight profile, the climb out stage is 305.9 m, which indicates that the missile is still under power roughly 13 m into its terminal flight stage. After powered flight, the missile is gliding on momentum and drag is the major force affecting it. Knowing it has a total flight time of roughly 14 seconds, the missile meets the minimum range of 2,000 m.

4. CONCLUSION

The main objective of this project was to analyze and design the launch and flight motors of the FGM-148 Javelin missile. The motor burn simulator BurnSim and COMSOL finite element analysis software were used to aid in the validation of design methods.

The spreadsheet derived from the example problem was validated with BurnSim. There was roughly an 18% error in magnitude between the thrust curves generated between the two methods. As the exact equations used by BurnSim to produce its thrust curve cannot be determined and what degree of rounding was done, the error was found to be acceptable. It was more important to note that overall curves were a match.

The launch motor was designed to be powerful and quick burning. This is needed in order to overcome the inertia of the missile from a standstill to a safe distance away from the launcher and at the same time burn out before exiting the tube. From Table 6, it is shown that a tubular propellant cross-section (using HTPB/AP/Al propellant) can produce the sufficient amount of thrust (~3,000 N) and burn out before the nozzle of the missile exits the launch tube. COMSOL FEM analysis verified that the pressure generated by the motor would not exceed the yield strength of the case.

The flight motor was designed to produce enough thrust to reach the maximum flight velocity of Mach .6 before burning out. Tables 8 and 9, show that the design produced by this project matches the performance of the actual missile. One difference that was found during the design is that the thrust curves of the project missile did not match the curve produced using actual thrust data. When the flight motor was designed to produce an equivalent maximum thrust at the time instance to the actual motor, it was found that it was insufficient to propel the missile to the required distance of 2 km. When the motor was designed to produce the same maximum thrust, but burn for the same amount of time as the actual motor, it was found that the missile would travel the required distance. COMSOL FEM analysis again verified that the pressure generated by the motor would not exceed the yield strength of the case.

The actual design of the burst disk could not be found, but the analysis of the burst disk with the assumed shape was found to be sufficient to withstand the large pressure (16 MPa) generated by the almost explosive combustion of the launch motor. The

pressure pushes aluminum almost to its breaking point, allowing the lower initial pressure (4 MPa) of the flight motor to break through the disk.

The soft launch-to-flight design of the Javelin missile was a very innovative design to allow a large and heavier missile to be launched by an individual. In addition, the incorporation of the two motors as a single unit with a burst disk allows the missile to remain compact enough to be portable.

REFERENCES

[1] Ward, T., *Aerospace Propulsion Systems*. First ed. (John Wiley & Sons Asia, 2010), 152-160

[2] Harris, J., Slegers, N., *Performance of a fire-and-forget anti-tank missile with a damaged wing*. (Mechanical and Aerospace Engineering Department, University of Alabama), 298

[3] Javelin Medium Antiarmor Weapon System Field Manual http://www.militarynewbie.com/pubs/FM@203-22.37%20Javelin%20Medium%20Antiarmor%20Weapon%20System.pdf

[4] Schön, Joakim., *Coefficient of friction and wear of a carbon fiber epoxy matrix composite*. (Swedish Defense Research Agency, 2003), Abstract

[5] Javelin Launch Tube Assembly (LTA) Brochure http://www.atk.com/products/documents/Javelin%20LTA.pdf

[6] Bruckart, James E., *Analysis of Injury Severity Caused by Flight Motor Overpressure of the Javelin Antiarmor Missile*. (United States Army Aeromedical Research Laboratory), 5

[7] Ward, T., *Aerospace Propulsion Systems*. First ed. (John Wiley & Sons Asia, 2010), 505-506

[8] Fleeman, E. L., *Tactical Missile Design*. (American Institute of Aeronautics and Astronautics, Inc.), 103 – 106

[9] Lyons, J., Long, D., Chait, R., *Critical Technology Events in the Development of the Stinger and Javelin Missile Systems*. (Center for Technology and National Security Policy, National Defense University), 25

[10] Headquarters Department of the Army, *FM 3-22 37 "Javelin Medium Antiarmor Weapon System"*. (2003)

[11] Miller, S., *Lift, Drag and Moment of a NACA 0015 Airfoil*. (Dept. of Aerospace Engineering, Ohio State University), 13

[12] Ward, T., *Aerospace Propulsion Systems*. First ed. (John Wiley & Sons Asia, 2010), Appendix A, Table A.1

[13] FIM-43 Rockeye http://en.wikipedia.org/wiki/FIM-43_Redeye

APPENDIX

SPREADSHEET VALIDATION VIA BurnSim SOFTWARE

Before the spreadsheet tool can be used to design the motors, its outputs must be validated. The tool was created based on an example problem from a propulsion text [1] with solutions. The example problem is an end burning motor, so the tool was converted to do a radial burning motor instead. The output of the spreadsheet is a thrust versus time graph. The same given information is used to start the BurnSim simulation. The example problem is in SI units and BurnSim runs in Imperial units, so a conversion had to be done. A driving propellant variable that was not readily available is the burn rate coefficient of Vielle's Law, which is found by converting all the known inputs to Imperial (Equation 19).

$$r_{b} = a\left(10^{-5}P_C\right)^{n}, \quad r_b \, in \frac{m}{s}, \quad k \, in \frac{m}{s}, \quad P_C \, in \, Pa$$
$$r_{b} = .013\, a\left(10^{-5}P_C\right)^{n}, \quad r_b \, in \frac{in}{s}, \quad k \, in \frac{m}{s}, \quad P_C \, in \, Pa \tag{19}$$

When the thrust curve BurmSim produces matches the thrust curve computed manually, the software can be considered validated and appropriate for further analytical use. BurnSim allows for the export of the output data points via a .csv file, which can be read and plotted by Excel (Fig. 11), after converting from Imperial to SI.

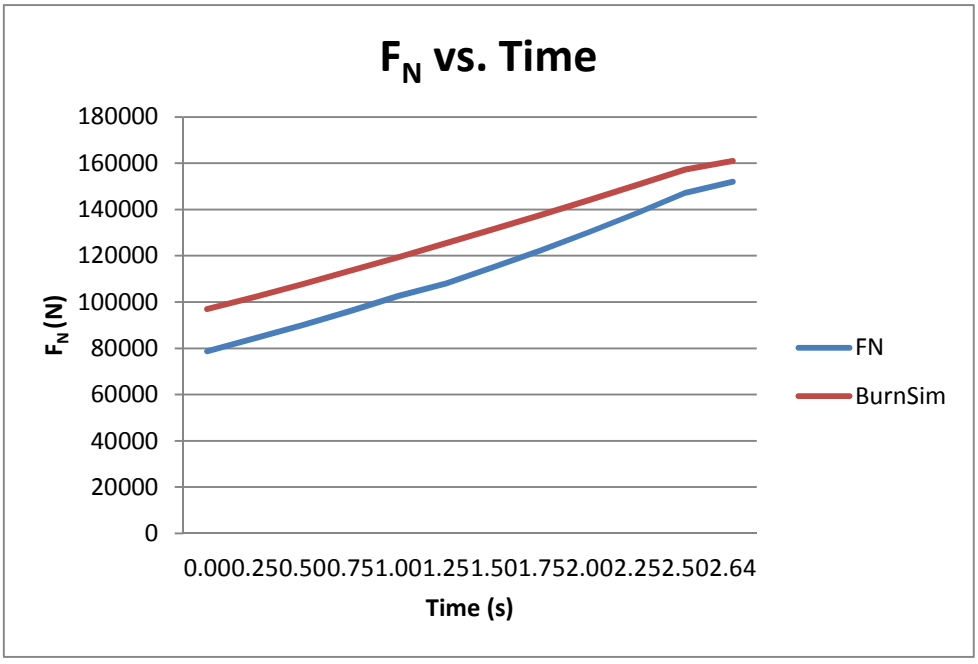

Figure 11: Analytical Spreadsheet vs. BurnSim Thrust Plot

The plot shows that the BurnSim result is roughly 18% higher than the analytical results. This disparity could be attributed to both rounding going from SI to Imperial, and the assumptions BurnSim makes, which are unknown as the source code is not available. However, as the trend between the two methods agrees for a radial burning, tube motor, it can be assumed that the spreadsheet tool is valid and can be used to design the motors.